Transient quantum evolution of two-dimensional electrons under photoexcitation of a deep center

F. T. Vasko*
Institute of Semiconductor Physics, NAS Ukraine, Praspekt Nauki 41, Kiev 03028, Ukraine

A. Hernandez-Cabrera† and P. Aceituno
Dpto. Fisica Basica, Universidad de La Laguna, La Laguna, 38206 Tenerife, Spain

(Received 4 September 2007; revised manuscript received 7 December 2007; published 11 February 2008)

We have considered the ballistic propagation of the two-dimensional (2D) electron Wigner distribution, which is excited by an ultrashort optical pulse from a deep center into the first quantized subband of a selectively doped heterostructure with high mobility. Transient ionization of a local state into a continuum conduction band state is described. Since the quantum nature of the photoexcitation, the Wigner distribution over 2D plane appears to be an alternating-sign function. Due to the negative contribution of the Wigner function, the mean values (concentration, energy, and flow) demonstrate an oscillating transient evolution in contrast to the diffusive classical regime of propagation.

DOI: 10.1103/PhysRevB.77.075310 PACS number(s): 73.20.−r, 05.30.−d, 78.47.−p

I. INTRODUCTION

In recent decades, intensive efforts were paid in order to study the quantum coherent properties of different physical systems.[1] During the development of the ultrafast spectroscopy of bulk semiconductors and heterostructures,[2] both coherent oscillations between coupled states and different relaxation processes have been investigated (see Refs. 3 and 4). Some quantum peculiarities (e.g., in the transport of carriers in mesoscopic devices[5] or in the dynamics of electrons excited at metallic surfaces[6]) were discussed recently. However, to the best of our knowledge, the coherent dynamics of a free quasiparticle, which propagates over continuum states, has not been measured directly in any solid state system. The quantum process of quasiparticle formation in different systems[7–10] has been observed for subpicosecond stage of evolution. Under the theoretical consideration of such a kind of measurements (see, for example, Ref. 11 and references therein), one can model the photogeneration process using a simple initial condition to describe the creation of carriers during a femtosecond temporal interval. At the same time, in the case of photoexcitation of carriers with low concentration and with energy values below the optical phonon energy, the collisionless regime of the response appears to be valid up to a nanosecond time interval. This is because both the fast relaxation, due to optical phonon emission, and the carrier-carrier interaction are suppressed. Thus, a possibility is to study the quantum nature of the ballistic transient evolution, caused by the nonclassical character of photoexcitation.[4,12]

Modern high-mobility heterostructures are characterized by a momentum relaxation time shorter than nanoseconds at low temperatures.[13] So that the mean free path appears to be macroscopic (>100 μm if the electron energy is about few meVs). The photoexcitation of a single deep center under a laser pumping focused up to submicron scale[14] can be carried out in a nondoped heterostructure with a low surface concentration of centers [deep centers in bulk GaAs are under consideration since the 1970s (Refs. 15)]. Below, we consider the transient photoexcitation of electrons from a deep local level and the quantum ballistic evolution of the Wigner distribution in the two-dimensional (2D) plane over submillimeter distances during a nanosecond time interval.

In contrast to the transitions between local states, when the Rabi effect (oscillations of population versus pumping intensity[4,12]) takes place, the level population of a deep center state under ultrafast photoionization decreases monotonically with the pumping intensity due to the delocalization of the excited electron over the conduction c band. Another peculiarity of the process under consideration is the quantum character of the transient evolution of the distribution excited into the continuous spectrum. Due to this, the concentration distribution, which decreases from the center, involves an oscillating contribution and there are regions where the Wigner distribution takes negative values. Such a distribution should be considered with the use of the quantum kinetic equation, written in the Wigner representation, due to the following reasons: (a) the energy conservation law is not valid during the photoexcitation process and (b) there is no momentum restrictions on the excited distribution due to the short-range local state involved in the phototransition.

In this paper, we restrict ourselves to the local time approximation, which corresponds to the photoionization above the c-band edge ($\Delta\omega\tau_{ex}>1$, where τ_{ex} is the duration of the photoexcitation and $\Delta\omega$ is the detuning frequency with respect to the photoionization energy), when only point (b) is essential. Due to the violation of the momentum conservation law, the mean values (concentration, energy, and flow) show an oscillating behavior in contrast to the diffusive classical regime. Moreover, although the concentration and energy distributions are positive functions, the flow distribution is an alternating-sign one, i.e., the flow may be directed opposite to the concentration gradient. The peculiarities discussed can be verified by means of optical methods or scanning tunneling microscopy, if the measurements can be performed with submicron and subnanosecond resolutions.

The present work is organized as follows. The photoexcitation process, including the evolution of the deep center population and the transient Wigner distribution over c band, is described in Sec. II. Section III presents the temporal dependencies of the above-introduced functions. The transient dynamics of the mean values is described in Sec. IV. A list of the assumptions used and the discussion of the methods for

experimental verification of the peculiarities discussed are given in the concluding section. Appendix contains the description of the classical regime of transient evolution under a smooth interband excitation.

II. ULTRAFAST PHOTOEXCITATION

Under photoexcitation of electrons, transitions from a deep local level into the first subband of c band is described by the density matrix $\hat{\rho}_{jt}$, where the index j means c band or local state. Performing the averaging over the period of the radiation $\mathbf{E}_t \exp(-i\omega t)+\text{c.c.}$, one obtains the quantum kinetic equation,[12]

$$\frac{\partial \hat{\rho}_{jt}}{\partial t} + \frac{i}{\hbar}[\hat{h}_j, \hat{\rho}_{jt}] = \hat{G}_{jt}, \tag{1}$$

with the generation rate $(j \neq j')$,

$$\hat{G}_{jt} = \left(\frac{e}{\hbar\omega}\right)^2 \int_{-\infty}^{t} dt' e^{-i\omega(t'-t)} \times \{\hat{S}^{+}_{jt'-t}(\mathbf{E}_{t'}\cdot\hat{\mathbf{v}})_{jj'}\hat{\rho}_{j't'}\hat{S}_{j't'-t}(\mathbf{E}_t\cdot\hat{\mathbf{v}}^{+})_{j'j} + (\mathbf{E}_t\cdot\hat{\mathbf{v}}^{+})_{jj'}\hat{S}^{+}_{j't'-t}\hat{\rho}_{j't'}(\mathbf{E}_{t'}\cdot\hat{\mathbf{v}})_{j'j}\hat{S}_{jt'-t}\}_{j\neq j'} + \text{H.c.} \tag{2}$$

Here, $\hat{h}_j$ is the Hamiltonian of the 2D state in the c band $(j=c)$ or of the state at short-range center $(j=h)$, $\hat{S}_{jt'-t}=\exp[-i\hat{h}_j(t'-t)/\hbar]$ is the evolution operator of the jth state, and $(\hat{\mathbf{v}})_{jj'}$ is the velocity matrix element for $j \leftrightarrow j'$ transitions. For the case of a deep center connected to the valence v band,[16] we use in Eq. (2) the interband matrix element of velocity v_{cv} multiplied by the overlap integral between the plane wave of momentum $\mathbf{p}$ and the local state $I_{\mathbf{p}}=\langle \mathbf{p}|h\rangle$. The evolution of the Wigner distribution function over the c band, $f_{\mathbf{p}_1,\mathbf{p}_2,t}=\langle \mathbf{p}_1|\hat{\rho}_{ct}|\mathbf{p}_2\rangle$, is governed by the equation

$$\frac{\partial f_{\mathbf{p}_1,\mathbf{p}_2,t}}{\partial t} + \frac{i}{\hbar}(\varepsilon_{p_1}-\varepsilon_{p_2})f_{\mathbf{p}_1,\mathbf{p}_2,t} = G_{\mathbf{p}_1,\mathbf{p}_2,t},$$

$$G_{\mathbf{p}_1,\mathbf{p}_2,t} \simeq \left(\frac{eEv_{cv}}{\hbar\omega}\right)^2 I_{\mathbf{p}_1} I^{*}_{\mathbf{p}_2} w_t \int_{-\infty}^{t} dt' w_{t'} e^{i(\varepsilon_{p_2}/\hbar-\Delta\omega)(t'-t)} n_{t'} + (\text{c.c.}, \mathbf{p}_1 \leftrightarrow \mathbf{p}_2), \tag{3}$$

with the right-hand side dependent on the population of the local state, $n_t \equiv \langle h|\hat{\rho}_{ht}|h\rangle$. The generation rate $G_{\mathbf{p}_1,\mathbf{p}_2,t}$ is determined through the 2D kinetic energy $\varepsilon_p=p^2/m$, with the effective mass of the c band m, the form factor w_t, introduced by the relation $\mathbf{E}_t=\mathbf{E}w_t$, and the detuning energy, $\hbar\Delta\omega$.

We are using the initial conditions $f_{\mathbf{p}_1,\mathbf{p}_2,t\to-\infty}=0$ and $n_{t\to-\infty}=1$, which correspond to the single-electron population of the local level, so that the normalization condition takes the form $n_t+2\Sigma_{\mathbf{p}} f_{\mathbf{p},\mathbf{p},t}=1$. The evolution of the local state population is governed by the integrodifferential equation,

$$\frac{dn_t}{dt} + 2\left(\frac{eEv_{cv}}{\hbar\omega}\right)^2 w_t \int_{-\infty}^{t} dt' w_{t'} n_{t'} \times \sum_{\mathbf{p}} |I_{\mathbf{p}}|^2 \cos\left(\frac{\varepsilon_p}{\hbar}-\Delta\omega\right)(t-t') = 0, \tag{4}$$

which is obtained from Eqs. (1) and (2). Instead of Eq. (3), one can describe the transient evolution of the c-band distribution through the Wigner function, $f_{\mathbf{p},\mathbf{q},t} \equiv f_{\mathbf{p}-\hbar\mathbf{q}/2,\mathbf{p}+\hbar\mathbf{q}/2,t}$, which is governed by the equation

$$\left(\frac{\partial}{\partial t} + i\mathbf{q}\cdot\mathbf{v}\right) f_{\mathbf{p},\mathbf{q},t} = G_{\mathbf{p},\mathbf{q},t}, \tag{5}$$

with the velocity $\mathbf{v}=\mathbf{p}/m$. Similarly, the generation rate $G_{\mathbf{p},\mathbf{q},t} \equiv G_{\mathbf{p}-\hbar\mathbf{q}/2,\mathbf{p}+\hbar\mathbf{q}/2,t}$ is transformed into

$$G_{\mathbf{p},\mathbf{q},t} \simeq \left(\frac{eEv_{cv}}{\hbar\omega}\right)^2 I_{\mathbf{p}+\hbar\mathbf{q}/2} I_{\mathbf{p}-\hbar\mathbf{q}/2} w_t \int_{-\infty}^{t} dt' w_{t'} n_{t'} \times \left\{\exp\left[i\left(\frac{\varepsilon_{\mathbf{p}+\hbar\mathbf{q}/2}}{\hbar}-\Delta\omega\right)(t'-t)\right] + (\text{c.c.}, \mathbf{q}\to-\mathbf{q})\right\}, \tag{6}$$

and the right-hand side of Eq. (5) is determined through the evolution of n_t. The solution of Eq. (5) takes the form $f_{\mathbf{p},\mathbf{q},t} = \int_{-\infty}^{t} dt' \exp[-i\mathbf{q}\cdot\mathbf{v}(t-t')] G_{\mathbf{p},\mathbf{q},t'}$, so the description of the transient evolution is reduced to the calculation of a multiple integral and to the solution of Eq. (4).

A simplified consideration of the problem is possible under the condition $\Delta\omega\tau_{ex}>1$ (photoionization into a high-energy state of the c band) when $w_{t'}n_{t'}$ in Eqs. (4) and (6) can be replaced by $w_t n_t$ due to the fast oscillating factors (the local time approximation). The integration over dt' in Eq. (6), which is performed with an infinitesimal damping factor in the exponent, $\delta \to +0$, gives

$$G_{\mathbf{p},\mathbf{q},t} \approx \left(\frac{eEv_{cv}}{\hbar\omega}\right)^2 I_{\mathbf{p}+\hbar\mathbf{q}/2} I_{\mathbf{p}-\hbar\mathbf{q}/2} w_t^2 n_t \times \left[\frac{\hbar/i}{\varepsilon_{\mathbf{p}+\hbar\mathbf{q}/2}-\hbar\Delta\omega-i\delta} + (\text{c.c.}, \mathbf{q}\to-\mathbf{q})\right]. \tag{7}$$

Here, the kinetic energy of the inhomogeneous system $(\mathbf{q}\neq 0)$ is not conserved during the photogeneration process, even for the long τ_{ex} case, due to the violation of the momentum conservation law. Using Eq. (7) and performing the Fourier transformation of the distribution function $f_{\mathbf{p},\mathbf{q},t}$, one obtains

$$f_{\mathbf{p},\mathbf{x},t} = \sum_{\mathbf{q}} \int_{-\infty}^{t} dt' e^{i\mathbf{q}\cdot\mathbf{x}_{t-t'}} G_{\mathbf{p},\mathbf{q},t'} \approx 2\hbar\left(\frac{eEv_{cv}}{\hbar\omega}\right)^2 \int_{-\infty}^{t} dt' w_{t'}^2 n_{t'} \sum_{\mathbf{q}} I_{\mathbf{p}+\hbar\mathbf{q}/2} I_{\mathbf{p}-\hbar\mathbf{q}/2} \times \left[\pi\delta(\varepsilon_{\mathbf{p}+\hbar\mathbf{q}/2}-\hbar\Delta\omega)\cos(\mathbf{q}\cdot\mathbf{x}_{t-t'}) + \frac{\sin(\mathbf{q}\cdot\mathbf{x}_{t-t'})}{\varepsilon_{\mathbf{p}+\hbar\mathbf{q}/2}-\hbar\Delta\omega}\right], \tag{8}$$

where we have introduced the time-dependent coordinate,

$\mathbf{x}_{t-t'}=\mathbf{x}-\mathbf{v}(t-t')$. The function $f_{\mathbf{p},\mathbf{x},t}$ satisfies the conditions $f_{-\mathbf{p},-\mathbf{x},t}=f_{\mathbf{p},\mathbf{x},t}$ and $f_{-\mathbf{p},\mathbf{x},t}=f_{\mathbf{p},-\mathbf{x},t}$, which are verified by the exchange $\mathbf{q}\rightarrow-\mathbf{q}$ in Eq. (8).

Within the local time approximation, Eq. (4) takes the form

$$\left(\frac{d}{dt}+\gamma w_t^2\right)n_t=0,$$

$$\gamma=4\pi\left(\frac{eEv_{cv}}{\hbar\omega}\right)^2\sum_{\mathbf{p}}|I_{\mathbf{p}}|^2\delta(\varepsilon_p/\hbar-\Delta\omega), \tag{9}$$

where γ stands for the photoionization decrement. The analytical solution of Eq. (9),

$$n_t=1-\gamma\int_{-\infty}^{t}dt'w_{t'}^2\exp\left(-\gamma\int_{t'}^{t}dt''w_{t''}^2\right), \tag{10}$$

describes the transient population of the level.[17] Thus, we have obtained the Wigner distribution [Eq. (8)] and the population [Eq. (10)] written in the integral forms which include the overlap integral $I_{\mathbf{p}}$ and the form factor w_t.

III. SHORT-RANGE CASE

To calculate the Wigner distribution [Eq. (8)] and the population [Eq. (10)], we use below the overlap integral for the short-range local state with the characteristic size l_o, so that $I_{\mathbf{p}}\simeq l_o/L$ if $p<\hbar/l_o$ and $I_{\mathbf{p}}$ tends to zero if $p>\hbar/l_o$; here, L is the normalization length. Within the above assumption, the decrement of photoionization in Eq. (9) takes the form

$$\gamma\simeq\left(\pi\frac{eEv_{cv}}{\hbar\omega}l_o\right)^2\hbar\rho_{2D}=\frac{\pi^3 m}{2m_h}\left(\frac{eEv_{cv}}{\hbar\omega}\right)^2\frac{\hbar}{\Delta E}, \tag{11}$$

where ρ_{2D} is the density of states, m_h is the heavy hole mass, and the level coupling energy ΔE is expressed through l_o according to $\Delta E\simeq(\hbar/l_o)^2/2m_h$. The temporal dependencies of n_t under different pumping levels, which are determined by the dimensionless parameter $\gamma\tau_{ex}/2$, are shown in Fig. 1 for the Gaussian form factor $w_t=\exp[-2(t/\tau_{ex})^2]$. The complete ionization of the center appears under the condition $\gamma\tau_{ex}/2\sim2$ and, when γ increases, the photoionization takes place during the front of the pulse. The full ionization regime takes place under a pulse energy of ~0.2 μJ focused on an area of ~100 μm; this estimate is performed for the GaAs parameters and does not depend on the pulse duration.

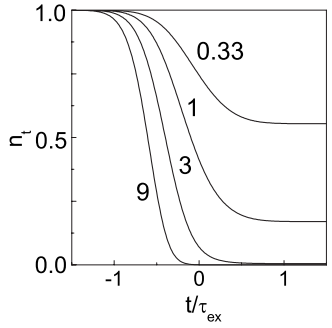

FIG. 1. Transient evolution of the population of the deep level under the dimensionless pumpings $\gamma\tau_{ex}/2=0.33$, 1, 3, and 9.

Next, we turn to the description of the photoexcited electron distribution given by Eq. (8) and dependent on time, $|\mathbf{p}|$, $|\mathbf{x}|$, and the angle $\hat{\mathbf{p},\mathbf{x}}$. We consider the long-duration excitation case (the collisionless regime of the response takes place for the nanosecond time scale) and demonstrate that the Wigner distribution $f_{\mathbf{p},\mathbf{x},t}$ is not a positive function. We calculate below the distribution at the maximal pumping, $t=0$, for the cases $\mathbf{p}\|\mathbf{x}$ and $\mathbf{p}\perp\mathbf{x}$ with the use of the notations $f_{p,x}^{\|}$ and $f_{p,x}^{\perp}$, respectively. Performing in Eq. (8) the integration over $\mathbf{q}\perp\mathbf{p}$, one obtains the distributions $f_{p,x}^{\|,\perp}$ as follows:

$$\left|\begin{matrix}f_{p,x}^{\|}\\ f_{p,x}^{\perp}\end{matrix}\right|=\frac{2\gamma}{\pi}\int_{-\infty}^{0}dtw_t^2n_t\int_{-\infty}^{\infty}dp_1\left\{\frac{\theta[p_{\Delta\omega}^2-p_1^2]}{\sqrt{p_{\Delta\omega}^2-p_1^2}}\left|\begin{matrix}\cos\left[\frac{2(p_1-p)}{\hbar}(x+vt)\right]\\ \cos\left[\frac{2x}{\hbar}\sqrt{p_{\Delta\omega}^2-p_1^2}+\frac{2(p_1-p)}{\hbar}vt\right]\end{matrix}\right|\right.$$
$$\left.+\frac{\theta[p_1^2-p_{\Delta\omega}^2]}{\sqrt{p_1^2-p_{\Delta\omega}^2}}\left|\begin{matrix}\sin\left[\frac{2(p_1-p)}{\hbar}(x+vt)\right]\\ \exp\left[-\frac{2x}{\hbar}\sqrt{p_1^2-p_{\Delta\omega}^2}\right]\sin\left[\frac{2(p_1-p)}{\hbar}vt\right]\end{matrix}\right|\right\}, \tag{12}$$

where $\theta[z]$ is the Heaviside step function, $v=|\mathbf{v}|$, and $p_{\Delta\omega}=\sqrt{2m\hbar\Delta\omega}$ is the characteristic momentum. The integrals over t and p_1 can be factorized for the slow electron case, $p\simeq0$; moreover, a nonzero contribution appears from the first addendum only. The distributions for the $\|$ and $\perp$ orientations are coincident,

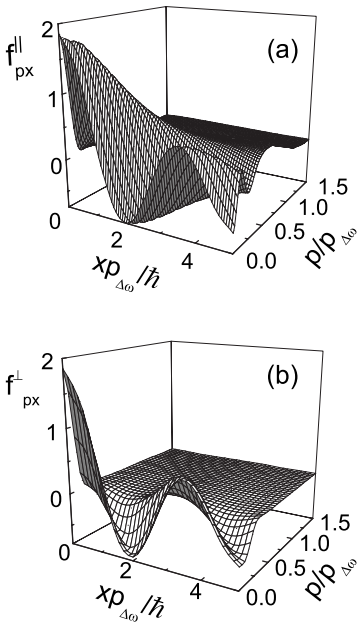

FIG. 2. (a) Longitudinal and (b) transverse Wigner distributions at maximal pumping ($t=0$) versus dimensionless momentum and coordinate, $p/p_{\Delta\omega}$ and $xp_{\Delta\omega}/\hbar$. Parameters used are $\Delta\omega\tau_{ex}=10$ and $\gamma\tau_{ex}/2=3$, where $\tau_{ex}=0.66$ ps.

$$f^{\parallel,\perp}_{p=0,x} \simeq 2\gamma \int_{-\infty}^{0} dt w_t^2 n_t J_0\left(\frac{2p_{\Delta\omega}x}{\hbar}\right), \tag{13}$$

and the coordinate dependence is given by the zero-order Bessel function, $J_0(z)$, which has an alternating-sign value and decreases as a square root.

The distribution functions [Eq. (12)] depend on the dimensionless momentum and coordinate, $p/p_{\Delta\omega}$ and $xp_{\Delta\omega}/\hbar$, the detuning parameter $\Delta\omega\tau_{ex}$, and the pumping intensity γ. Using Eq. (10) with the dimensionless pumping $\gamma\tau_{ex}/2=3$ and performing the numerical integration in Eq. (12), we plot the Wigner distribution for $\Delta\omega\tau_{ex}=10$, as it is shown in Fig. 2. One can see a nonmonotonically dependence on $p/p_{\Delta\omega}$ and $xp_{\Delta\omega}/\hbar$ with pronounced negative contributions. Both longitudinal [Fig. 2(a)] and transverse [Fig. 2(b)] cases show a fast decrease with dimensionless momentum, although the first case is not as fast as the other: $f^{\parallel}_{p,x}$ becomes zero for $p/p_{\Delta\omega}\sim 1.5$, whereas for the transverse case, $p/p_{\Delta\omega}\sim 0.5$ is enough to get $f^{\perp}_{p,x}\simeq 0$ due to the exponential term in the denominator of Eq. (12). However, we have extended the dimensionless momentum axis up to 1.5 in Fig. 2(b) in order to directly compare with Fig. 2(a). Moreover, oscillations slowly decrease with dimensionless coordinate $xp_{\Delta\omega}/\hbar$ due to the spread of the distribution under propagation. However, as $p/p_{\Delta\omega}$ increases, the dependence on $xp_{\Delta\omega}/\hbar$ is opposite for the two cases considered: for the longitudinal case, peaks shift to higher $xp_{\Delta\omega}/\hbar$ values, whereas, in the other case, peaks move toward smaller $xp_{\Delta\omega}/\hbar$ values. In other words, propagations of the Wigner distribution are perpendicular in the phase space for the two cases under consideration.

IV. MEAN VALUES

The transient dynamics of this Wigner distribution can be verified by the treatment of spatiotemporal dependencies of the mean values (concentration, energy, and flow, $n_{\mathbf{x}t}$, $\mathcal{E}_{\mathbf{x}t}$, and $\mathbf{i}_{\mathbf{x}t}$, respectively) given by the standard formulas,

$$\begin{vmatrix} n_{\mathbf{x}t} \\ \mathcal{E}_{\mathbf{x}t} \\ \mathbf{i}_{\mathbf{x}t} \end{vmatrix} = 2\int \frac{d\mathbf{p}}{(2\pi\hbar)^2} \begin{vmatrix} 1 \\ \varepsilon_p \\ \mathbf{v} \end{vmatrix} f_{\mathbf{p},\mathbf{x},t}. \tag{14}$$

Below, we analyze the spatiotemporal evolution of Eq. (14) using distribution (8). Performing the integration over the variable $\mathbf{p}\pm\hbar\mathbf{q}/2$, one obtains the concentration and energy distributions, which are isotropic over the $\mathbf{x}$ plane,

$$\begin{vmatrix} n_{xt} \\ \mathcal{E}_{xt} \end{vmatrix} = \frac{\gamma}{2\pi}\int_{-\infty}^{t} dt' w_{t'}^2 n_{t'} \int_0^{\infty} dq J_0(qx) q \begin{vmatrix} N_{q,t-t'} \\ E_{q,t-t'} \end{vmatrix}. \tag{15}$$

Here, the kernels $N_{q,\tau}$ and $E_{q,\tau}$ are given by

$$N_{q,\tau} = \cos\left(\frac{\varepsilon_{\hbar q}\tau}{\hbar}\right) J_0(qv_{\Delta\omega}\tau) + \sin\left(\frac{\varepsilon_{\hbar q}\tau}{\hbar}\right)\mathcal{P}\int_0^{\infty} dy \frac{J_0(qv_{\Delta\omega}\tau\sqrt{y})}{\pi(y-1)} \tag{16}$$

and

$$\begin{aligned} E_{q,\tau} = {} & \cos\left(\frac{\varepsilon_{\hbar q}\tau}{\hbar}\right)\left(\hbar\Delta\omega + \frac{\varepsilon_{\hbar q}}{4}\right) J_0(qv_{\Delta\omega}\tau) \\ & + \sin\left(\frac{\varepsilon_{\hbar q}\tau}{\hbar}\right)\mathcal{P}\int_0^{\infty} dy \left(\hbar\Delta\omega y + \frac{\varepsilon_{\hbar q}}{4}\right)\frac{J_0(qv_{\Delta\omega}\tau\sqrt{y})}{\pi(y-1)} \\ & + \hbar q v_{\Delta\omega}\left[\cos\left(\frac{\varepsilon_{\hbar q}\tau}{\hbar}\right)\mathcal{P}\int_0^{\infty} dy\sqrt{y}\frac{J_1(qv_{\Delta\omega}\tau\sqrt{y})}{\pi(y-1)} \right. \\ & \left. - \sin\left(\frac{\varepsilon_{\hbar q}\tau}{\hbar}\right) J_1(qv_{\Delta\omega}\tau)\right], \end{aligned} \tag{17}$$

where $\mathcal{P}$ means the principal value of the integral, $J_1(z)$ is the first-order Bessel function, $v_{\Delta\omega}\equiv p_{\Delta\omega}/m$, and $y=\varepsilon/\hbar\Delta\omega$ is the dimensionless energy. The distributions [Eq. (15)] depend on the pumping intensity through n_t, given by Eq. (10), and on the dimensionless coordinate and time, $xp_{\Delta\omega}/\hbar$ and t/τ_{ex}.

Before numerical calculations, we consider the asymptotes of n_{xt} (similar formulas can be written for $\mathcal{E}_{xt}$ and the flow distribution) for the case $t\gg\tau_{ex}$ and $x\gg\hbar/p_{\Delta\omega}$. Using the asymptotic expansion of the Bessel function for large arguments and performing the integrations over t' and q, one obtains the explicit expression,

$$\begin{aligned} n_{xt} = {} & \frac{\gamma\tau_{ex}\mathcal{N}}{(2\pi)^2 l_{\Delta\omega}\sqrt{xv_{\Delta\omega}t}}\sqrt{\frac{\pi}{\Delta\omega t}}\left\{\sin\left(z_-^2+\frac{\pi}{4}\right) - \sin\left(z_+^2+\frac{\pi}{4}\right)\right. \\ & \left. + \mathcal{P}\int_0^{\infty}\frac{dy}{\pi\sqrt{y}(y-1)}\left[\cos\left(z_{y-}^2+\frac{\pi}{4}\right) - \sin\left(z_{y+}^2+\frac{\pi}{4}\right)\right]\right\}, \end{aligned} \tag{18}$$

where $\mathcal{N}=\int_{-\infty}^{\infty} dt w_t^2 n_t/\tau_{ex}$, $l_{\Delta\omega}=\hbar/p_{\Delta\omega}$, and we have introduced the dimensionless forms $z_{\pm}=(x\pm v_{\Delta\omega}t)p_{\Delta\omega}/2\hbar\sqrt{\Delta\omega t}$ and $z_{y\pm}=z_{\pm}\pm(\sqrt{y}-1)\sqrt{\Delta\omega t}$. Thus, the period of the oscilla-

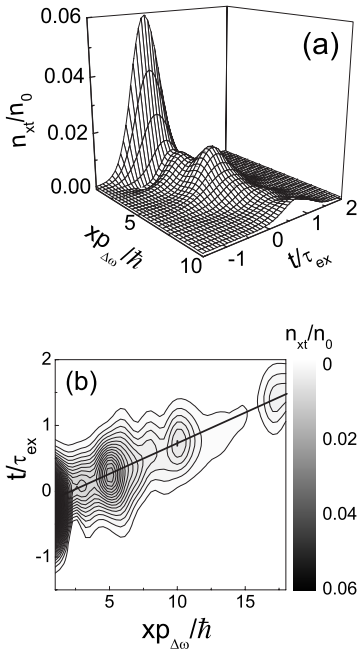

FIG. 3. Spatiotemporal evolution of concentration n_{xt}. (a) 3D graph near the peak and (b) contour plot showing the line corresponding to the classical velocity. Parameters used are $\Delta\omega\tau_{ex}=5$ and $\gamma\tau_{ex}/2=1$, where $\tau_{ex}=0.66$ ps.

tions of the concentration distribution, $(\hbar/2p_{\Delta\omega})\sqrt{\Delta\omega t}$, does not depend on $\Delta\omega$ and increases as $\sqrt{t}$.

The spatiotemporal dependence of the concentration is shown in Fig. 3. Figure 3(a) shows the three-dimensional (3D) graph near the peak at $xp_{\Delta\omega}/\hbar=0$ for $\Delta\omega\tau_{ex}=5$ and $\gamma\tau_{ex}/2=1$. As can be seen, concentration falls quickly for small dimensionless coordinate and oscillates for bigger $xp_{\Delta\omega}/\hbar$ values. In order to appreciate oscillations, we have removed $xp_{\Delta\omega}/\hbar<1$ values from the figure because of the high value of n_{xt} maximum at $x=0$. Position of n_{xt} maximum in dimensionless time is shifted following the classical velocity, as shown in Fig. 3(b), where the contour plot, together with the line corresponding to the classical velocity, is presented. Concentration is normalized by $n_0=\gamma\tau_{ex}m\Delta\omega/\pi\hbar$, which is equal to 2.82×10^{11} cm^{-2} for $\hbar\Delta\omega=5$ meV, and $\gamma\tau_{ex}/2=1$. This value corresponds to an excited electron localized over an area of the order of $(\hbar/p_{\Delta\omega})^2$.

Figure 4 shows the behavior of the energy distribution vs dimensionless position and time. Energy distribution has been normalized by $\mathcal{E}_0=n_0\hbar\Delta\omega$, which corresponds to 2.25×10^{-3} erg/cm^2 for the same values of $\hbar\Delta\omega$ and $\gamma\tau_{ex}/2$ used for the concentration. Energy behavior vs $xp_{\Delta\omega}/\hbar$ is similar to the concentration one. To say, a fast decrease followed by oscillations. As in the former figure, we have removed $xp_{\Delta\omega}/\hbar<2$ values from the figure because of the high value of $\mathcal{E}_{xt}$ maximum at $x=0$.

Since the in-plane isotropy of the problem, one obtains the flow density $\mathbf{i}_{\mathbf{x}t}=(\mathbf{x}/|\mathbf{x}|)I_{xt}$, where the scalar function I_{xt} takes a similar form to Eq. (15),

$$I_{xt}=\frac{\gamma}{2\pi}\int_{-\infty}^{t}dt'w_{t'}^2n_{t'}\int_0^\infty dqJ_1(qx)qF_{q,t-t'}, \tag{19}$$

with the kernel

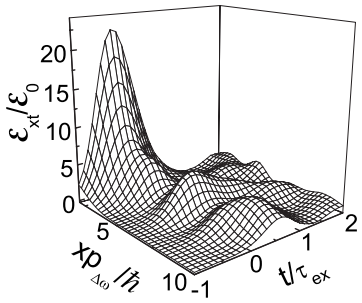

FIG. 4. Evolution of energy $\mathcal{E}_{xt}$ for the same parameters of Fig. 3.

$$F_{q,\tau}=\frac{\hbar q}{2m}\left[\cos\left(\frac{\varepsilon_{\hbar q}\tau}{\hbar}\right)\mathcal{P}\int_0^\infty dy\frac{J_0(qv_{\Delta\omega}\tau\sqrt{y})}{\pi(y-1)}-\sin\left(\frac{\varepsilon_{\hbar q}\tau}{\hbar}\right)J_0(qv_{\Delta\omega}\tau)\right]-v_{\Delta\omega}\left[\cos\left(\frac{\varepsilon_{\hbar q}\tau}{\hbar}\right)J_1(qv_{\Delta\omega}\tau)-\sin\left(\frac{\varepsilon_{\hbar q}\tau}{\hbar}\right)\mathcal{P}\int_0^\infty\frac{dy\sqrt{y}}{\pi(y-1)}J_1(qv_{\Delta\omega}\tau\sqrt{y})\right]. \tag{20}$$

Performing the numerical integrations given by Eqs. (19) and (20), we plot the flow distribution for the above parameters, as it is shown in Fig. 5. Flow distribution has also been normalized by $I_0=n_0p_{\Delta\omega}/m$, being $I_0=4.57\times10^{18}$ (cm/s)/cm^2 for the above values of $\hbar\Delta\omega$ and $\gamma\tau_{ex}/2$. The flow is identically zero at $xp_{\Delta\omega}/\hbar=0$, having a sharp peak for $xp_{\Delta\omega}/\hbar<1$, followed by oscillations in dimensionless coordinate, as shown in Fig. 5(a). Only the de-

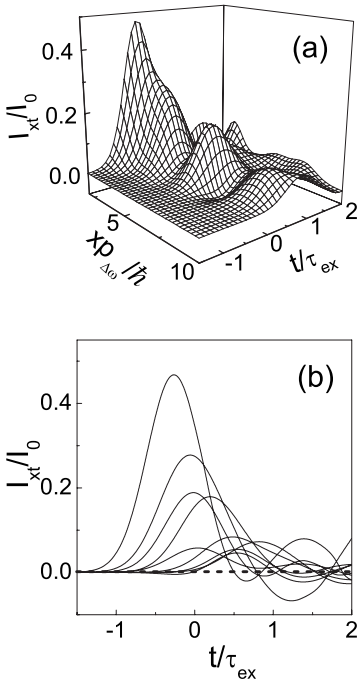

FIG. 5. Evolution of the flow I_{xt} (a) for the same parameters of Fig. 3. (b) Curves for some $xp_{\Delta\omega}/\hbar$ values in order to show negative part of the flow.

scending slope of the peak appears in the figure because dimensionless distance axis starts at 2. We have opted for starting at this point because the high value of the first maximum would prevent to see the flow fluctuations. Moreover, as can be seen, there are also oscillations in time and negative values of the flow distribution arise. With the purpose of showing negative parts of flow, we represent in Fig. 5(b) the flow vs dimensionless time for different $xp_{\Delta\omega}/\hbar$ values (from 2 to 10).

V. CONCLUSIONS

In summary, we have suggested a scheme to investigate the quantum peculiarities of the single-particle dynamics under ultrafast photoionization of a single deep center. Due to the negative contributions to the transient Wigner distribution of the c-band electron, the mean values (concentration, energy, and flow) demonstrate an oscillatory behavior in contrast to the classical results (see Appendix). We have analyzed the conditions for visible quantum oscillations, when an experimental mapping of the Wigner distribution should be possible through the character of these oscillations.

Now, we turn to the discussion of possibilities for experimental verification of the peculiarities obtained. The stage of selective single-electron photoexcitation is based on the assumption of a low concentration of deep centers: if a bulk concentration less than 10^{12} cm^{-3} remains in the near-surface region, one obtains an intercenter distance about 1 μm. The regime of a single-center excitation can be easily realized with an ultrafast pump focused over a submicron scale. Recently, similar measurements were performed with a single quantum dot[18] but the photoexcitation into continuum and further evolution of the distribution was not examined. Perhaps, it is due to the complicate problem of the registration of the oscillating Wigner distribution. In spite of the sensitive optical methods developed recently for optical control of a single quantum dot (see Refs. 19 and 20 and references therein), the spatial resolution remains a complicate task (we use above $\hbar/p_{\Delta\omega}\sim 10$ nm). Note that the period of the oscillations increases with time as $\sqrt{t}$ [see Eq. (18) and Fig. 3(b)] but the distribution value (and the response) decreases due to spatial spread. Another possibility is to use the scanning tunneling microscopy[21] which has nanometer resolution but has to be adapted to time-resolved measurements with subnanosecond resolution. Note that we do not calculate any concrete optical or tunneling response supposing that the observed peculiarities will be of the same order of the mean values considered in Sec. IV.

Next, we discuss the assumptions used in our calculations. The main approximation is the local time approach, so that the edge photoexcitation is beyond of our consideration. A more complicate numerical simulation is required for this case as well as to take into account the Coulomb correlations (excitonic effect). The interaction of the electron with the localized hole is essential for a near-center region but it should decrease with x. Thus, the short-range model used in our calculations of Eqs. (9) and (11) is enough in order to estimate the photoionization decrement. Finally, only the averaged Wigner distribution has been considered and a full counting statistics of photoionization and subsequent transient propagation of electrons[22] requires a special investigation.

In conclusion, a similar theoretical analysis may be developed for other cases like photoexcitation of a single quantum dot or near-field photoexcitation,[14,18] where a similar quantum behavior should take place. We hope these results will stimulate experimental efforts toward a mapping of quantum peculiarities in the transient Wigner distribution.

ACKNOWLEDGMENTS

This work has been supported in part by Ministerio de Educación y Ciencia (Spain) and FEDER under Project No. FIS2005-01672 and by FRSF of Ukraine (Grant No. 16/2).

APPENDIX A: CLASSICAL EVOLUTION

This appendix contains the description of the classical regime of transient evolution when the momentum and coordinate dependences of the generation rate can be factorized in contrast to Eq. (7). Such a regime appears for a smooth interband excitation, with the inhomogeneity scale l_{ex} exceeds $\hbar/\sqrt{2m\varepsilon_{ex}}$, where ε_{ex} is the excitation energy. Following Sec. 53 of Ref. 12, we approximate the generation rate by the factorized expression,

$$G_{\mathbf{p},\mathbf{q},t} \propto \delta_{\Delta\varepsilon}(\varepsilon-\varepsilon_{ex})e^{-(ql_{ex})^2}w_t^2. \tag{A1}$$

Here, $\delta_{\Delta\varepsilon}(\varepsilon-\varepsilon_{ex})$ is the peak energy distribution with the half-width $\Delta\varepsilon$ and w_t is the above-introduced form factor. After the integration over the $\mathbf{q}$ plane, the distribution $f_{\mathbf{p},\mathbf{x},t}$ takes the form

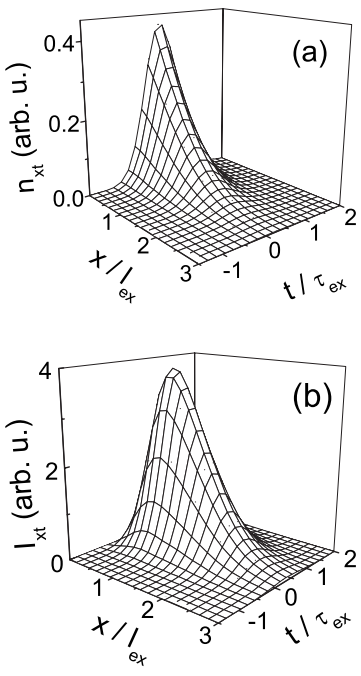

FIG. 6. Evolution of the classical distributions (a) n_{xt} and (b) I_{xt} given by Eqs. (A3) and (A4) for $\alpha=6$.

$$f_{\mathbf{p},\mathbf{x},t} \propto \delta_{\Delta\varepsilon}(\varepsilon - \varepsilon_{ex}) \int_{-\infty}^{t} dt' w_{t'}^2 \exp\left[-\frac{1}{2}\left(\frac{\mathbf{x}_{t-t'}}{l_{ex}} \right)^2 \right], \tag{A2}$$

so $f_{\mathbf{p},\mathbf{x},t} > 0$ because of the positive functions under the integral. At $t \gg \tau_{ex}$, one obtains the distribution as a moving Gaussian peak: $f_{\mathbf{p},\mathbf{x},t} \propto \delta_{\Delta\varepsilon}(\varepsilon - \varepsilon_{ex}) \exp[-(1/2)(\mathbf{x}_t/l_{ex})^2]$. The explicit expressions for $f_{p,x}^{\parallel,\perp}$ introduced in analogy to Eq. (12) can be written through the probability integrals and they have a single-peak behavior.

Restricting ourselves to a narrow energy distribution, $\Delta\varepsilon \ll \varepsilon_{ex}$, and taking the integrals over $\mathbf{p}$ plane according definition (14), one obtains the concentration distribution as follows:

$$n_{xt} \propto \exp\left[-\frac{1}{2}\left(\frac{x}{l_{ex}} \right)^2 \right] \int_{-\infty}^{t/\tau_{ex}} d\tau e^{-4\tau^2} \times e^{-\alpha(t/\tau_{ex} - \tau)^2} I_0\left[\alpha \frac{x}{l_{ex}} \left(\frac{t}{\tau_{ex}} - \tau \right) \right], \tag{A3}$$

where $I_0(z)$ is the zero-order Bessel function of imaginary argument. Here, we have introduced the dimensionless parameter $\alpha = v_{ex}\tau_{ex}/l_{ex}$, with $v_{ex} = \sqrt{2\varepsilon_{ex}/m}$. Within the above approximation, the energy distribution is given by $\mathcal{E}_{xt} \simeq \varepsilon_{ex} n_{xt}$. Similar to Eqs. (19) and (20), one obtains the flow density $\mathbf{i}_{\mathbf{x}t} = (\mathbf{x}/|\mathbf{x}|) I_{xt}$, where the scalar function I_{xt} is written as follows:

$$I_{xt} \propto v_{ex} \exp\left[-\frac{1}{2}\left(\frac{x}{l_{ex}} \right)^2 \right] \int_{-\infty}^{t/\tau_{ex}} d\tau e^{-4\tau^2} \times e^{-\alpha(t/\tau_{ex} - \tau)^2} I_1\left[\alpha \frac{x}{l_{ex}} \left(\frac{t}{\tau_{ex}} - \tau \right) \right]. \tag{A4}$$

where $I_1(z)$ is the first-order Bessel function of imaginary argument.

Performing a simple numerical integration of Eqs. (A3) and (A4), one obtains the concentration and flow distributions versus the dimensionless coordinate and time, x/l_{ex} and t/τ_{ex}, as it is shown in Fig. 6 for $\alpha = 6$. Since there are no oscillations of the classical distribution [Eq. (A2)], the mean values appear to be spread monotonically.

*ftvasko@yahoo.com
†ajhernan@ull.es

[1] M. Shapiro and P. Brumer, Phys. Rep. **425**, 195 (2006); W. S. Warren, H. Rabitz, and M. Dahleh, Science **259**, 1581 (1993).
[2] J. Shah, *Ultrafast Spectroscopy of Semiconductors and Semiconductor Nanostructures* (Springer, Heidelberg, 1999).
[3] *Nonequilibrium Physics at Short Time Scales*, edited by K. Morawetz (Springer, Heidelberg, 2004), Part III.
[4] V. M. Axt and T. Kuhn, Rep. Prog. Phys. **67**, 433 (2004).
[5] M. Nedjalkov, D. Vasileska, D. K. Ferry, C. Jacoboni, C. Ringhofer, I. Dimov, and V. Palankovski, Phys. Rev. B **74**, 035311 (2006); M. Nedjalkov, H. Kosina, S. Selberherr, C. Ringhofer, and D. K. Ferry, *ibid.* **70**, 115319 (2004).
[6] P. Lazic, V. M. Silkin, E. V. Chulkov, P. M. Echenique, and B. Gumhalter, Phys. Rev. Lett. **97**, 086801 (2006); B. Gumhalter, Phys. Rev. B **72**, 165406 (2005).
[7] R. Huber, F. Tauser, A. Brodschelm, M. Bichler, G. Abstreiter, and A. Leitenstorfer, Nature (London) **414**, 286 (2001).
[8] R. A. Kaindl, M. A. Carnahan, D. Hagele, R. Lovenich, and D. S. Chemla, Nature (London) **423**, 734 (2003).
[9] M. Hase, M. Kitajima, A. M. Constantinescu, and H. Petek, Nature (London) **426**, 51 (2003).
[10] R. Huber, C. Kübler, S. Tübel, A. Leitenstorfer, Q. T. Vu, H. Haug, F. Köhler, and M.-C. Amann, Phys. Rev. Lett. **94**, 027401 (2005).
[11] M. Herbst, M. Glanemann, V. M. Axt, and T. Kuhn, Phys. Rev. B **67**, 195305 (2003); T. Wolterink, V. M. Axt, and T. Kuhn, *ibid.* **67**, 115311 (2003).
[12] F. T. Vasko and O. E. Raichev, *Quantum Kinetic Theory and Applications* (Springer, New York, 2005).
[13] P. J. Burke, I. B. Spielman, J. P. Eisenstein, L. N. Pfeiffer, and K. W. West, Appl. Phys. Lett. **76**, 745 (2000).
[14] U. Neuberth, L. Walter, G. von Freymann, B. DalDon, H. Kalt, M. Wegener, G. Khitrova, and H. M. Gibbs, Appl. Phys. Lett. **80**, 3340 (2002); Y. Yayon, A. Esser, M. Rappaport, V. Umansky, H. Shtrikman, and I. Bar-Joseph, Phys. Rev. Lett. **89**, 157402 (2002); T. Guenther, V. Emiliani, F. Intonti, C. Lienau, T. Elsaesser, R. Nötzel, and K. H. Ploog, Appl. Phys. Lett. **75**, 3500 (1999).
[15] N. M. Kolchanova, I. D. Loginova, and I. N. Yassievich, Fiz. Tverd. Tela (Leningrad) **25**, 1650 (1983) [Sov. Phys. Solid State **25**, 952 (1983)]; N. M. Kolchanova, M. A. Sipovskaya, and Y. S. Smetannikova, Sov. Phys. Semicond. **16**, 1418 (1982).
[16] V. I. Perel and I. N. Yassievich, Zh. Eksp. Teor. Fiz. **87**, 237 (1982) [Sov. Phys. JETP **55**, 143 (1982)].
[17] Note that the particle conservation law, $(d/dt)(2\Sigma_{\mathbf{p}} f_{\mathbf{p},\mathbf{q}=0,t} + n_t) = 0$, can be verified under calculation of the time derivative of $2\Sigma_{\mathbf{p}} f_{\mathbf{p},\mathbf{q}=0,t}$ with the use of Eqs. (8) and (9).
[18] T. Guenther, C. Lienau, T. Elsaesser, M. Glanemann, V. M. Axt, T. Kuhn, S. Eshlaghi, and A. D. Wieck, Phys. Rev. Lett. **89**, 057401 (2002); M. Wesseli, C. Ruppert, S. Trumm, H. J. Krenner, J. J. Finley, and M. Betz, Appl. Phys. Lett. **88**, 203110 (2006).
[19] Q. Q. Wang, A. Muller, P. Bianucci, C. K. Shih, M. T. Cheng, H. J. Zhou, and J. B. Han, Appl. Phys. Lett. **89**, 142112 (2006); Y. Wu, X. Li, L. M. Duan, D. G. Steel, and D. Gammon, Phys. Rev. Lett. **96**, 087402 (2006).
[20] S. Seidl, A. Högele, M. Kroner, K. Karrai, R. J. Warburton, J. M. Garcia, and P. M. Petroff, Phys. Status Solidi A **204**, 381 (2007); P. A. Dalgarno, J. McFarlane, B. D. Gerardot, R. J. Warburton, K. Karrai, A. Badolato, and P. M. Petroff, Appl. Phys. Lett. **89**, 043107 (2006).
[21] A. M. Yakunin, A. Yu. Silov, P. M. Koenraad, J. H. Wolter, W. Van Roy, J. De Boeck, J.-M. Tang, and M. E. Flatte, Phys. Rev. Lett. **92**, 216806 (2004); G. Mahieu, B. Grandidier, D. Deresmes, J. P. Nys, D. Stievenard, and Ph. Ebert, *ibid.* **94**, 026407 (2005).
[22] T. Fujisawa, T. Hayashi, and S. Sasaki, Rep. Prog. Phys. **69**, 759 (2006); D. A. Bagrets, Y. Utsumi, D. S. Golubev, and G. Schon, Fortschr. Phys. **54**, 917 (2006).